Supplementary Materials

Increasing ankle push-off work with a powered prosthesis does not necessarily reduce metabolic rate for transtibial amputees

Roberto E. Quesada[1], Joshua M. Caputo[1,2], and Steven H. Collins[1,3]

1. Department of Mechanical Engineering, Carnegie Mellon University, Pittsburgh, PA
2. Human Motion Technologies L.L.C., Pittsburgh, PA
3. Robotics Institute, Carnegie Mellon University, Pittsburgh, PA

S1. Supplementary Methods

S1.1 Description of the ankle-foot prosthesis emulator

We used an experimental ankle-foot prosthesis emulator to systematically vary ankle push-off in isolation from other prosthesis features. We previously described this system in detail, including complete designs and code (Caputo & Collins, 2014a). We provide a brief overview here.

The system has three main elements: (1) powerful off-board motor and controller, (2) a tether transmitting mechanical power and sensor signals, (3) a lightweight instrumented end-effector worn by the participant (Fig. S1). This division of components maximizes responsiveness and minimizes end-effector mass during treadmill walking.

A powerful, low-inertia electric motor and a high-speed, real-time controller provide off-board actuation. Motor voltage is regulated using an industrial motor drive with embedded velocity control. Desired motor velocity commands are generated using the real-time controller. The transmission consists of a Bowden cable with a coiled-steel outer conduit and synthetic inner rope. The cable causes minimal interference with normal leg motions (Caputo & Collins, 2014a).

Figure S1. Photograph of the ankle-foot prosthesis end-effector.

The Bowden cable transmission pulls on the pulley, sprocket, chain and leaf-spring, in series, producing an ankle plantarflexion torque between the frame and forefoot. The pulley–sprocket component magnifies transmission forces and allows direct measurement of spring deflection. A tensioning spring keeps the chain engaged. A pyramidal adapter attaches to the pylon worn by the user. A dorsiflexion spring comprised of rubber bands retracts the toe during leg swing. Fiberglass leaf springs provide series elasticity for ankle torque measurement and control. A separate leaf spring directly connected to the frame (not the toe) comprises the heel.

Prosthesis dimensions approximate those of an average human foot (Hawes & Sovak, 1994). The distance between the heel and the toe is 0.22 m. The heel is 0.07 m to the rear of the pylon. The ankle is 0.07 m from the ground plane during standing. The toe is 0.07 m wide and the heel is 0.04 m wide, slightly narrower than the typical human dimensions of 0.10 and 0.07 m, respectively. Rubber pads at the toe and heel contact points approximate the effects of the sole of a walking shoe. The prosthesis end-effector weighs 1.2 kg.

Ankle rotation and pulley rotation are measured with encoders. Ankle torque is computed based on measurements of spring displacement and ankle position using a calibrated model. During calibration trials the prosthesis is fixed upside down while masses of known weight are hung from the toe. A range of masses and ankle angles that span the expected operating conditions are applied. Ankle torque is then modeled as a function of ankle angle and prosthesis pulley angle, with coefficients that minimize squared error during regression.

Torque control is achieved using proportional feedback on torque error, with damping injection on motor velocity to improve stability and iteratively learned feedforward compensations to improve torque tracking (Zhang et al., 2015). A similar feedback control law is used to perform ankle position control during the swing phase of walking, substituting a position error for torque error and using a modified gain.

Prosthetic ankle joint work was regulated using impedance control in two phases. In each phase, joint torque was controlled as a function of ankle angle. The Dorsiflexion phase began at heel contact and lasted until the velocity of the ankle joint reversed direction, usually around 75% of the stance period, when the prosthesis switched into the Plantarflexion phase. Dorsiflexion phase behavior was constant across conditions, while the torque profile in the Plantarflexion phase was adjusted to achieve desired levels of net prosthesis work rate. This changed work production during ankle push-off without altering other aspects of prosthesis function. Nominal parameters were selected to emulate the behavior of the biological ankle during normal walking at the same speed, in the manner of Caputo & Collins (2014b).

Safety features limit the forces exerted by the prosthesis on the human user. Software places limits on the maximum commanded torque. An electrical plantarflexion limit switch and electrical buttons accessible to the subject and experimenter deactivate the motor when pressed. A transmission break-away, composed of an empirically determined number of loops of thin synthetic rope, provide a mechanical failsafe.

S1.2. Additional details of motion capture and inverse-dynamics analysis methods

Reflective markers were placed on the sacrum, left and right anterior superior iliac spine, left and right greater trochanter, medial and lateral epicondyles of the knee, medial and lateral malleoli of the ankle, third metatarsophalangeal joint of the toe, and posterior calcaneus of the heel. On the prosthesis-side limb, markers were placed in locations approximating these landmarks on the socket and prosthesis. With the prosthesis emulator, the medial and lateral aspects of the forefoot axis of rotation were used in place of the medial and lateral malleoli of the ankle.

Joint angles were calculated using a standard Euler angle approach. Segment reference frames were defined according to the position of bony landmarks and joint angles were extracted from the linear transformation matrix that described the rotation from one coordinate system to another.

The foot coordinate system was defined by markers at the medial and lateral malleoli of the ankle, the third metatarsophalangeal joint of the toe, and the posterior calcaneus of the heel. The primary axis of the foot segment was defined as the vector connecting the midpoint of the ankle markers to the ankle marker on right side of the body segment. For the left leg, this was the medial ankle marker and for the right leg this was the lateral ankle marker. The secondary axis was defined as the cross product of the primary vector with the vector from the heel to the toe markers. The tertiary axis was defined as the cross product of the primary and secondary axes.

The shank coordinate system was defined by markers at the medial and lateral malleoli of the ankle and the medial and lateral epicondyles of the knee. The primary axis of the shank segment was defined in the same manner as the primary axis of the foot segment: as the vector connecting the midpoint of the ankle markers to the ankle marker on the right side of the body segment. The secondary axis was defined as the cross product of the primary vector with a vector drawn from the center of the ankle markers to the center of the knee markers. The tertiary axis was defined as the cross product of the primary and secondary axes. Ankle plantarflexion-dorsiflexion angles and moments were calculated about the shared primary axis of the foot and shank. Note that this choice of a shared primary axis disallows the measurement of rotation of the foot relative to the shank in the frontal and coronal planes. We opted for simplified foot marker placements to improve marker tracking while capturing the sagittal ankle rotations accurately. This simplification has negligible impact on inverse dynamics analysis, because both the movement and rotational inertia of the foot about these axes is very small (de Lava, 1996). To obtain accurate measurements of all foot and ankle degrees of freedom would require substantially more markers and model assumptions.

The thigh coordinate system was defined by markers at the medial and lateral epicondyles of the knee and the trochanters of the left and right hips. The primary axis of the thigh segment was defined as the vector connecting the midpoint of the knee markers to the knee marker on the right side of the body segment. The secondary axis was defined as the cross product of the primary vector with a vector from the center of the knee markers to the hip marker. The tertiary axis was defined as the cross product of the primary and secondary axes. Knee flexion-extension angles and moments were calculated about the primary axis of the thigh.

The pelvis coordinate system was defined by markers placed on the left and right greater trochanters, sacrum, and left and right sides of the anterior superior iliac spine. The primary axis of the pelvis segment was defined as the vector connecting the midpoint of the hip markers to the hip marker on the right side of the body. The tertiary axis was defined as the cross product of the primary vector with the vector drawn from the sacrum to the midpoint of the anterior superior iliac spine markers. The secondary axis was defined as the cross product of the tertiary and primary axes. Hip flexion-extension angles and moments were calculated about the primary axis of the pelvis.

Joint angles and moments were later inverted, as necessary, to conform to standard gait analysis conventions (Winter, 1991): Ankle angles were defined as positive for dorsiflexion and negative for plantarflexion, and ankle moments were defined as positive for plantarflexion and negative for dorsiflexion; Knee angles were defined as positive for flexion and negative for extension, and knee moments were defined as positive for extension and negative for flexion; Hip angles were defined as positive for flexion and negative for extension, and hip moments were defined as positive for extension and negative for flexion. In all cases, zero joint angle was defined as the angle during quiet standing with the Prescribed prosthesis. In all cases, joint power was unchanged in the conversion to gait analysis conventions, with positive remaining positive.

S2 Supplementary Results

S2.1. Supplementary Data

Please find a file archive named Quesada_2016_SuppData.zip included as supplementary material online. This archive includes a Matlab data structure with mean data for all conditions, subjects and outcomes measured, including ground reaction forces, center-of-mass power, joint mechanics, prosthesis mechanics, electromyography, metabolic rate and preference. Included is a ReadMe file explaining the organization of the data structure. Researchers are encouraged to contact the corresponding author with any questions about how to access this data.

S2.2. Supplementary Figures

The enclosed supplementary figures present prosthesis ankle power measured using onboard sensors (Fig. S2), the torque-angle relationship for the prosthesis (Fig. S3), prosthesis-side knee power and work-rates during swing (Fig. S4), ground reaction forces (Fig. S5), flexion-extension mechanics for the intact-side joints (Fig. S6) and prosthesis-side joints (Fig. S7), three-dimensional joint and pelvis angles (Fig. S8), electromyography for the intact-side muscles (Fig. S9) and prosthesis-side muscles (Fig. S10), center-of-mass work rates for individual subjects (Fig. S11) and metabolic rate versus net prosthesis work rate for one subject on 10 separate data collection days (Fig. S12).

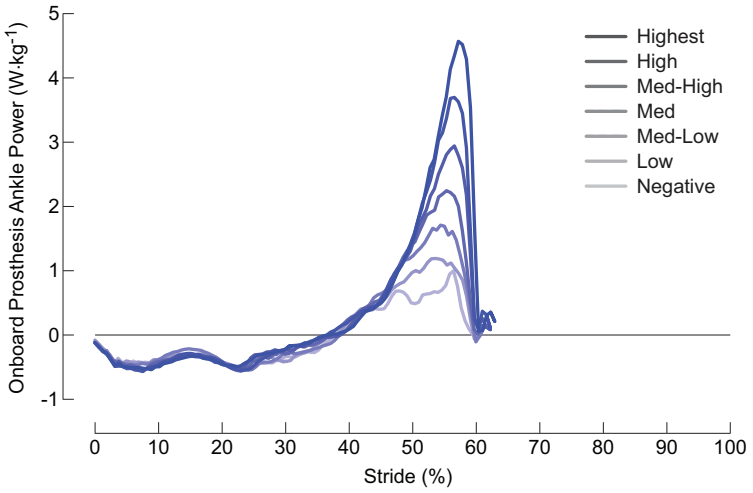

Figure S2: Prosthetic ankle joint power calculated based on onboard measurements of joint velocity and torque. Peak ankle power ranged from about half the value for Prescribed to about three times Prescribed. Patterns were similar to inverse-dynamics based power (cf. Fig. 2), but with less negative work during early and mid-stance, and without the burst of negative work just before push-off. Differences may relate to motion capture affect, filtering of motion capture data, or compliance in the prosthesis forefoot. This pattern of onboard joint power is similar to the patterns observed for other prostheses with active ankle push-off, such as the device reported by Au (2007; cf. Fig. 5-13), which tend to have less negative work in early and mid-stance and more rapid changes in power at the onset of push-off than measured for the same devices using inverse dynamics (Esposito et al., 2015). We provide both measurements to facilitate comparisons.

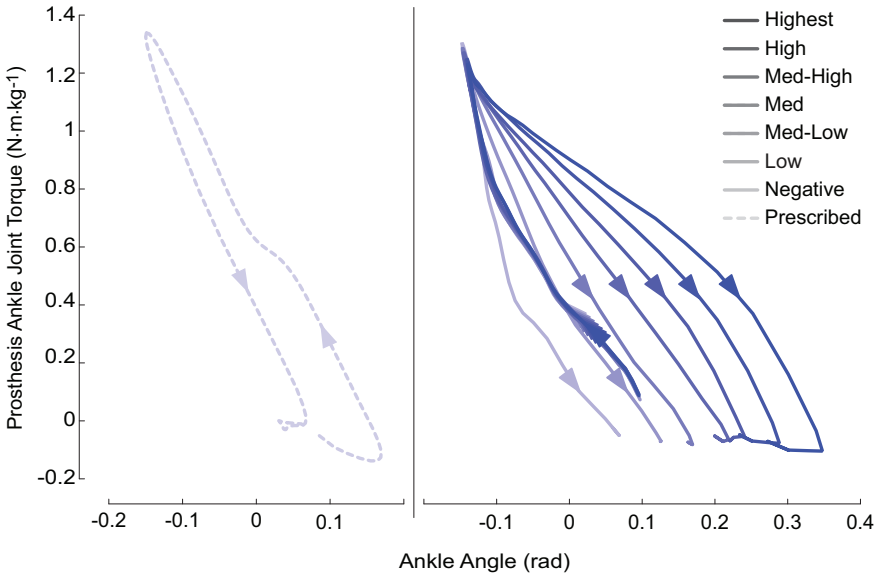

Figure S3: Prosthetic ankle joint torque versus joint angle measured using inverse dynamics (Prescribed, left) or onboard sensors (emulated, right). Progression in time is indicated by arrows. During walking with the Prescribed foot, a counterclockwise work loop was generated, indicating net absorption of energy by the prosthesis. During emulator conditions, work loops ranged from thin counterclockwise (Negative) to wide clockwise (Highest), indicating a large range of net energy absorption or production by the prosthesis. These work loops are similar to those reported for prior active prostheses (Herr & Grabowski, 2012), with the difference that the present results have a more circular, rather than dog leg shape, with a sharper corner at the top.

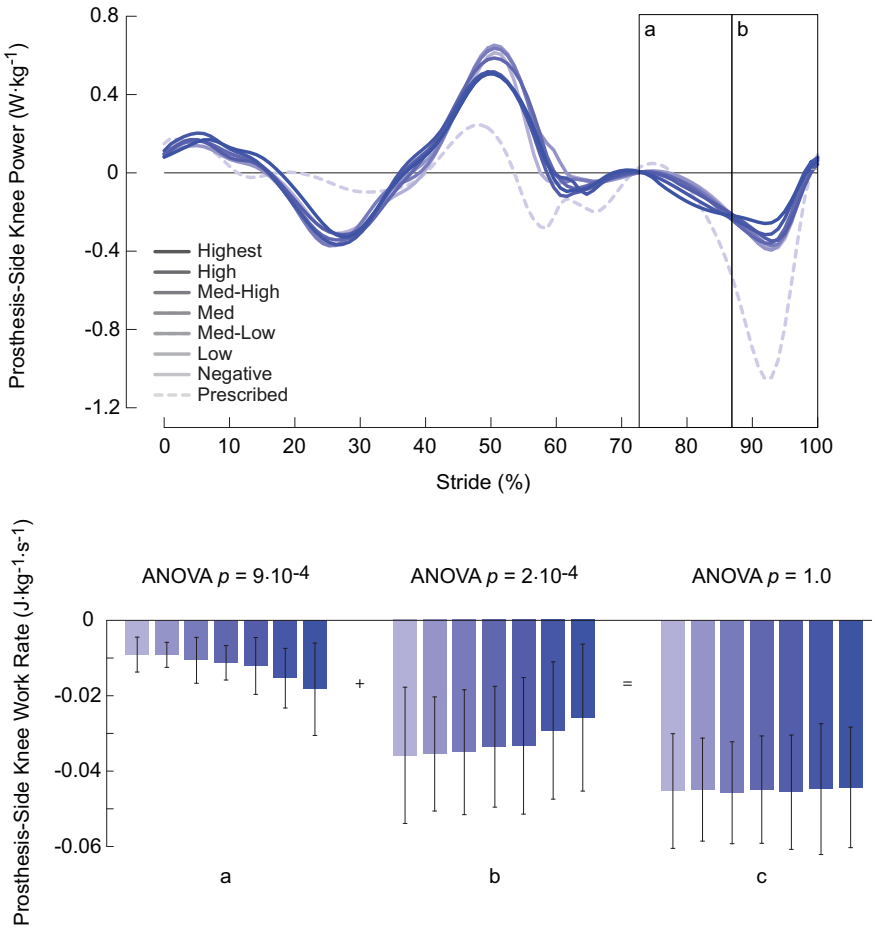

Figure S4: The pattern of prosthesis-side knee power (top) during swing was altered with increasing net prosthesis work rate. Mid-swing became more negative (a) while late swing became less negative (b). However, the total absorption during swing (c) was unchanged.

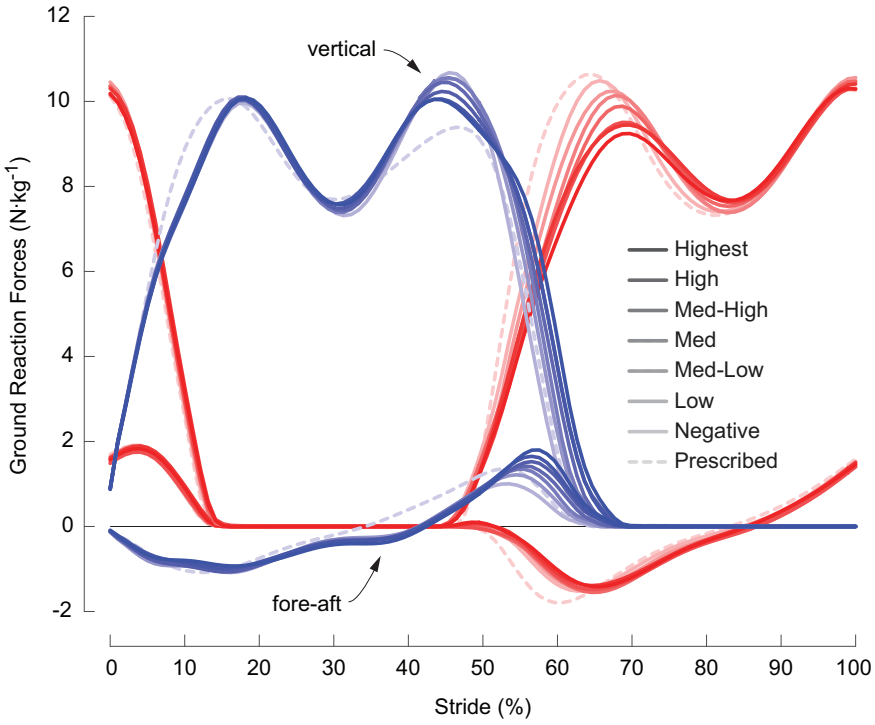

Figure S5: Vertical and fore-aft components of ground reaction force were strongly affected by prosthesis push-off work. As net prosthesis work rate increased, the peak vertical component of force during double-support decreased for both the prosthesis-side and intact-side limbs. The peak forward component of force on the prosthesis side increased, while the peak aftward force on the intact limb was unchanged. Vertical and fore-aft forces on the prosthesis side persisted longer, while peak vertical force in the intact limb occurred later. These trends are consistent with (and in fact completely determine) observed patterns in center-of-mass power (cf. Fig. 5).

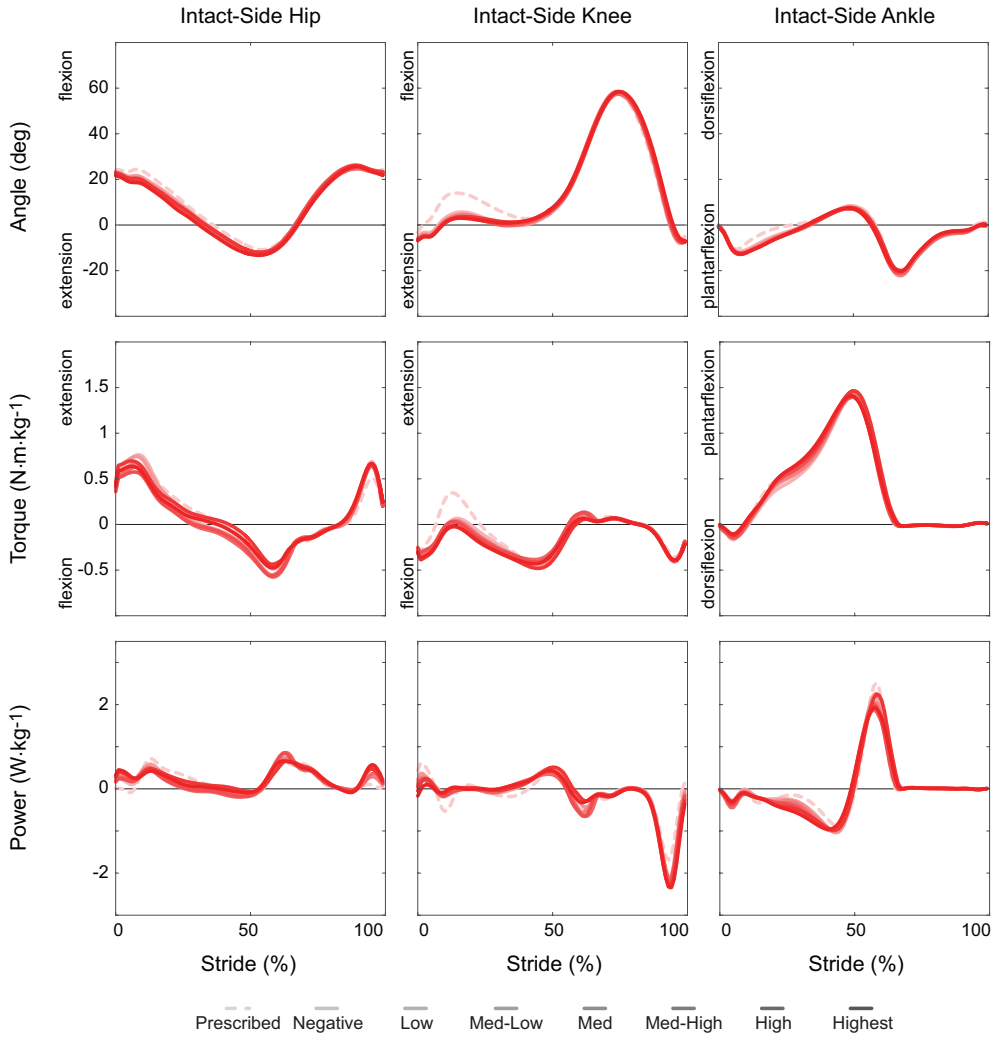

Figure S6: Intact-side flexion-extension joint mechanics, provided for reference. There were no apparent trends in intact-side joint mechanics. Zero joint angle corresponds to quiet standing with the Prescribed prosthesis. Trajectories begin with intact-side heel strike at 0% stride.

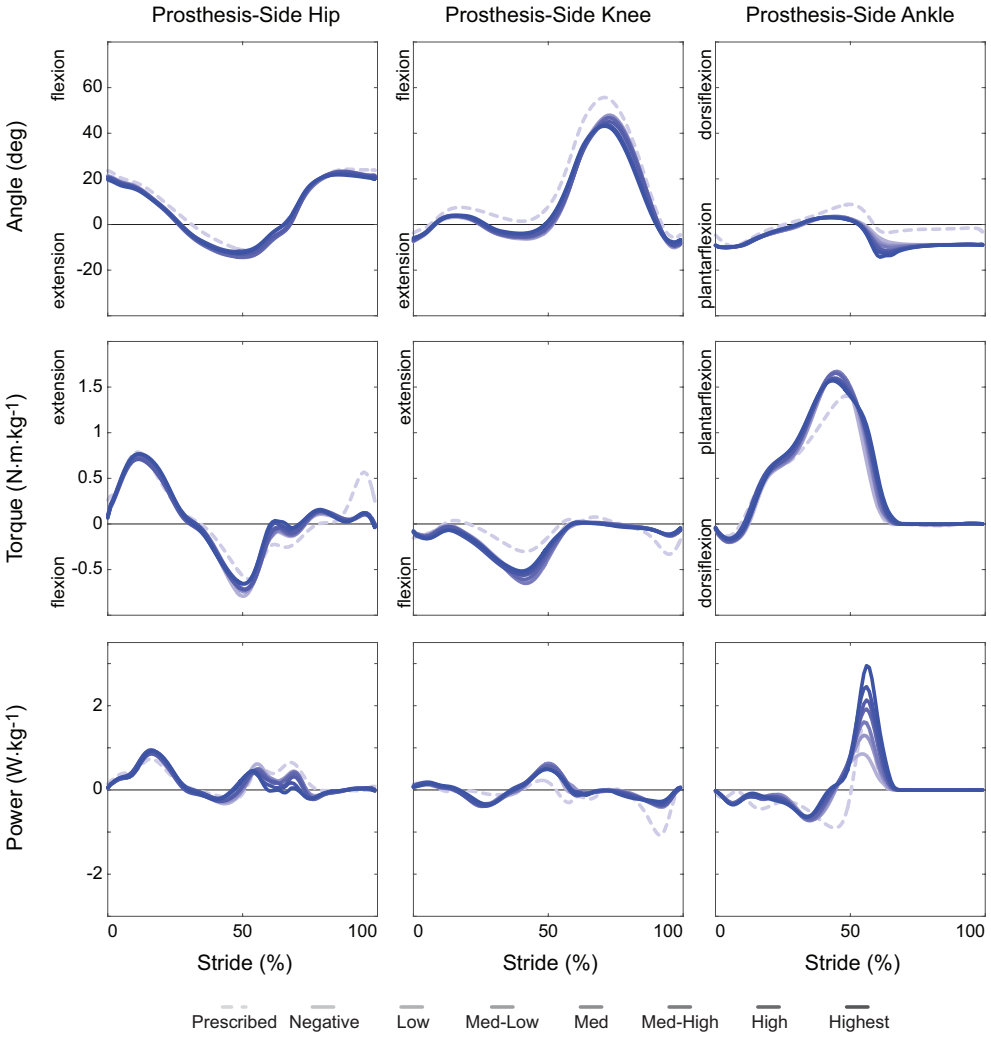

Figure S7: Prosthesis-side flexion-extension joint mechanics, provided for reference. Aside from prosthesis-side hip power (cf. Fig. 6), knee power (Fig. S4) and ankle power (cf. Fig. 2), there were no other apparent changes in prosthesis-side mechanics. Zero joint angle corresponds to quiet standing with the Prescribed prosthesis. Trajectories begin with prosthesis-side heel strike at 0% stride.

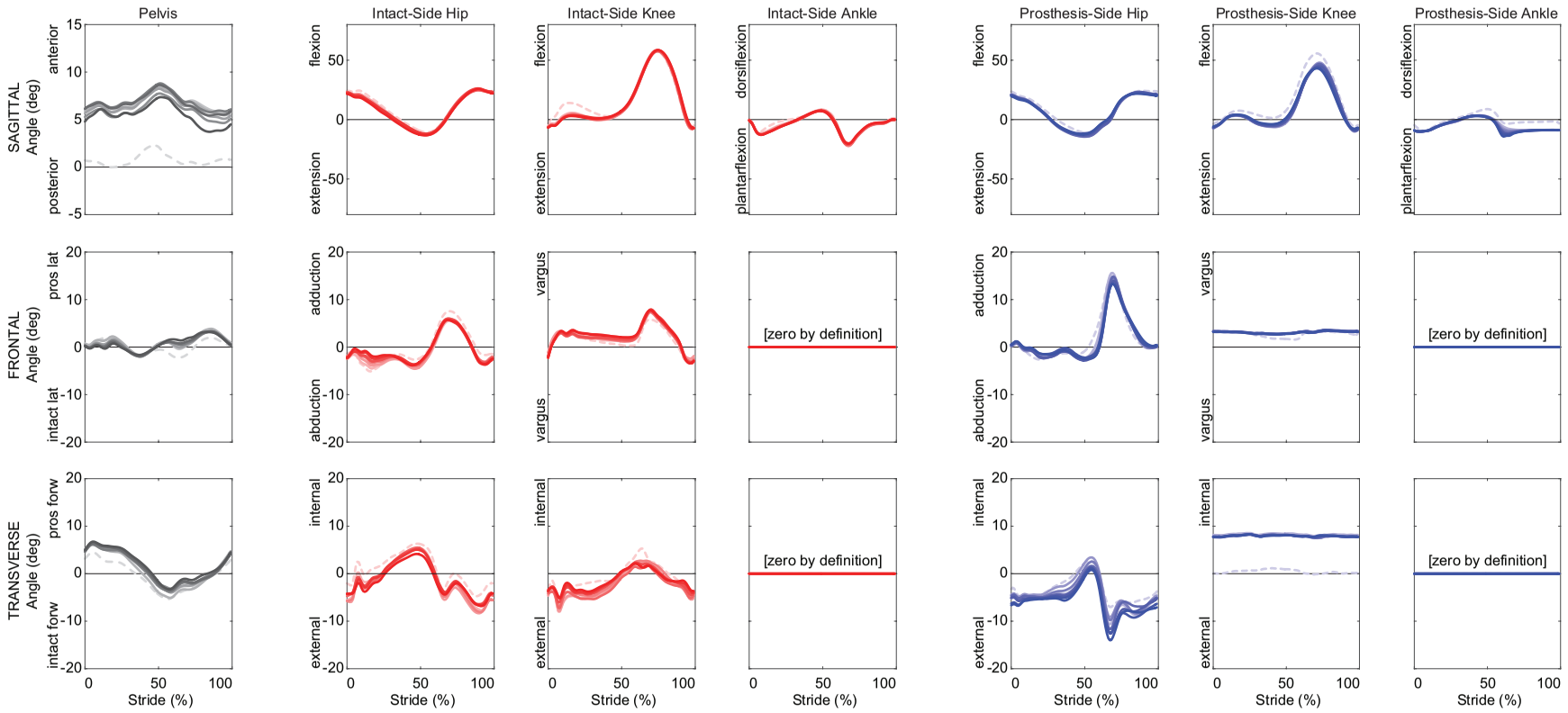

Figure S8: Three-dimensional joint and pelvis segment angles, provided for reference. Patterns of motion fall within ranges typical of clinical gait analysis for amputees. Pelvis trajectories begin with prosthesis-side heel strike at 0% stride, with positive and negative angles defined with respect to prosthesis (pros) position. Joint trajectories begin with ipsilateral heel strike at 0% stride, i.e. intact-side for intact joint data and prosthesis-side for prosthesis-side joint data. Hip adduction during swing across all conditions may be the result of relatively wide steps taken on the split-belt treadmill. Ankle rotations outside of plantarflexion-dorsiflexion were not captured using the local reference frames defined above, because our primary interest was plantarflexion-dorsiflexion of prosthetic structures with little frontal and coronal compliance.

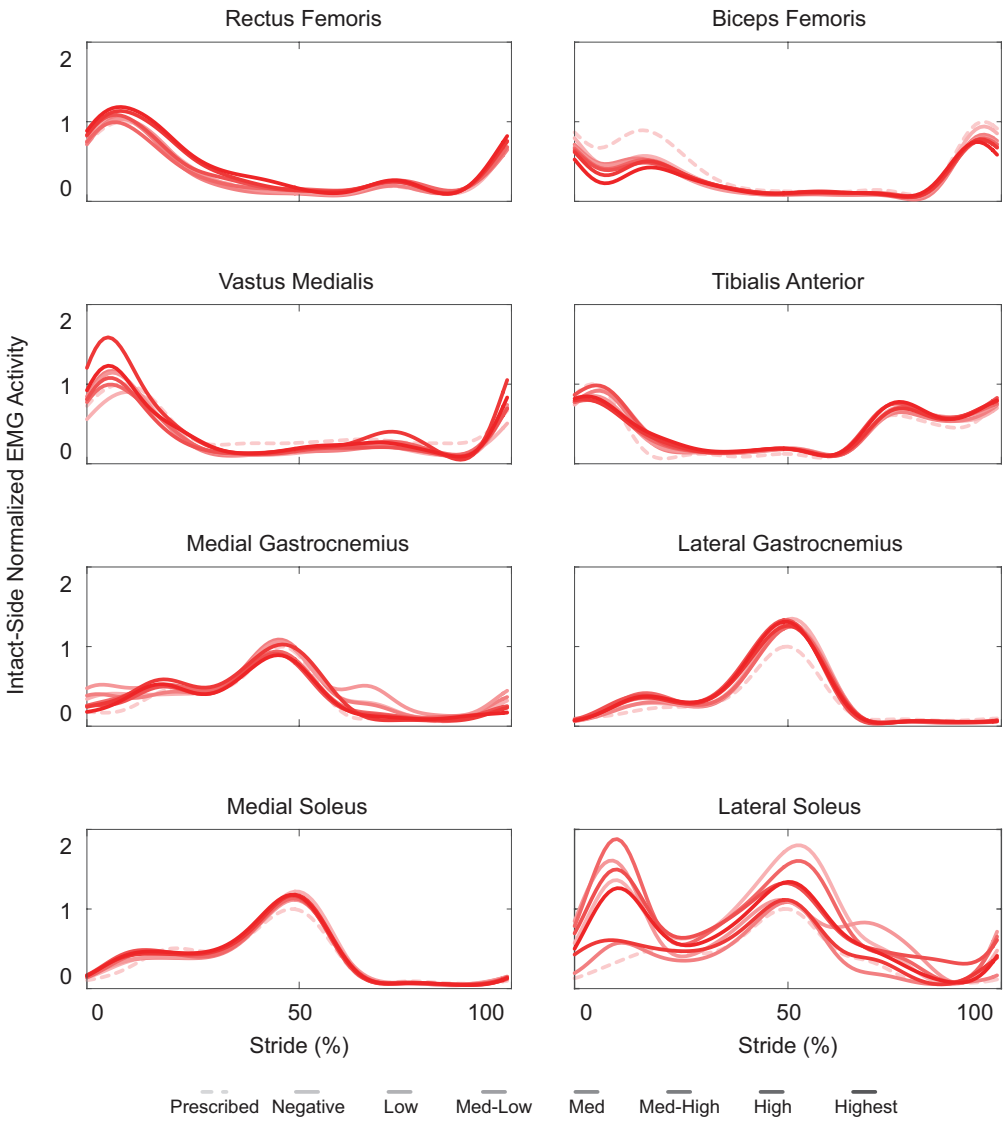

Figure S9: Intact-side electromyography, provided for reference. Aside from biceps femoris activity (cf. Fig. 8), trends were not observed for any muscles. Notably, while activity in the lateral soleus and vastus medialis were higher in some conditions than with the prescribed prosthesis, there was no clear effect of prosthesis work level. Such changes therefore do not seem to provide an explanation for the lack of reduction in metabolic rate with higher levels of prosthesis work. Trajectories begin with intact-side heel strike at 0% stride.

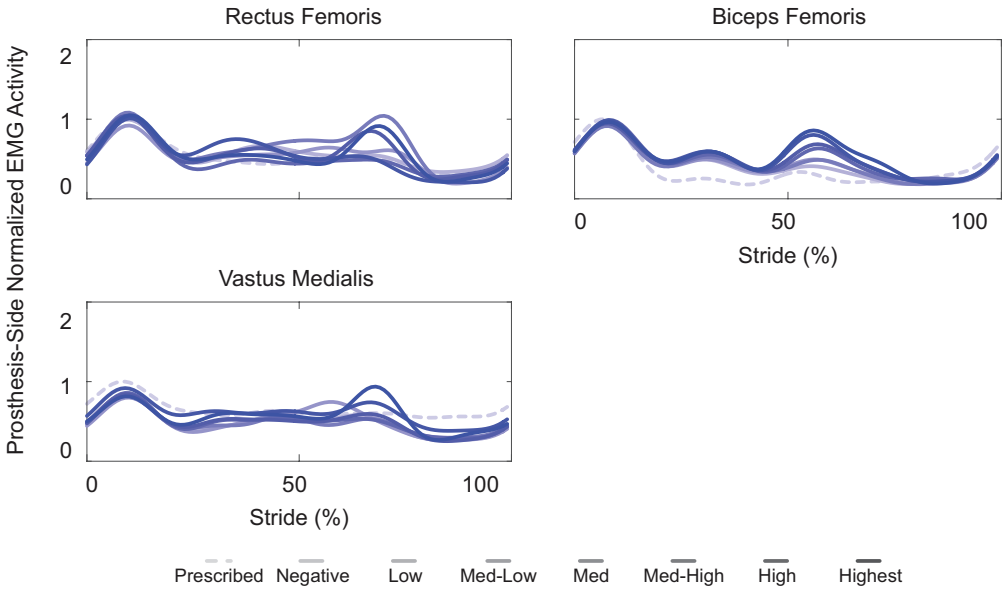

Figure S10: Prosthesis-side electromyography, provided for reference. Aside from biceps femoris (cf. Fig. 7), trends were not observed for any muscles. Trajectories begin with prosthesis-side heel strike at 0% stride.

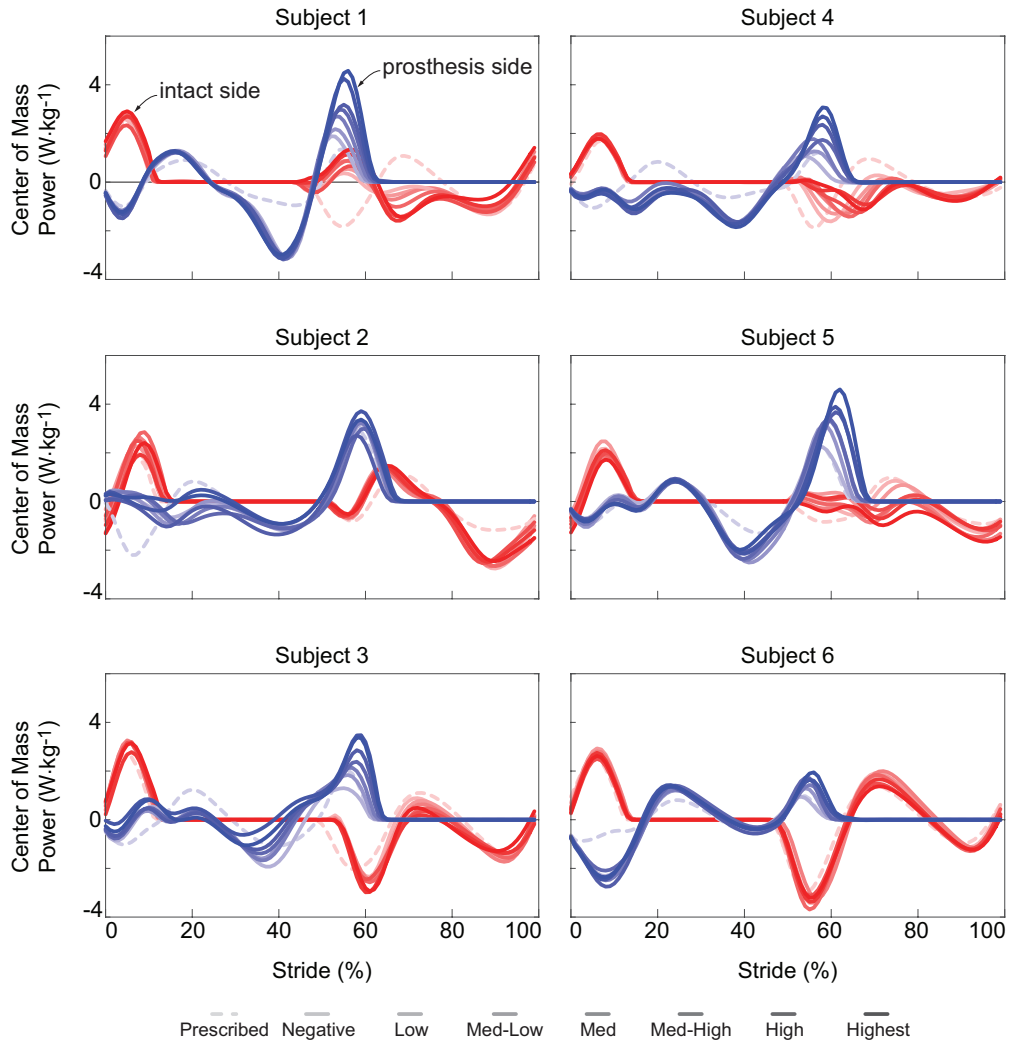

Figure S11: Center-of-mass power trajectories varied greatly between subjects. This variability makes it difficult to extend conclusions made during experiments on non-amputee populations, which are generally more uniform, to amputees. Red lines are intact-side trajectories, blue lines are prosthesis-side trajectories.

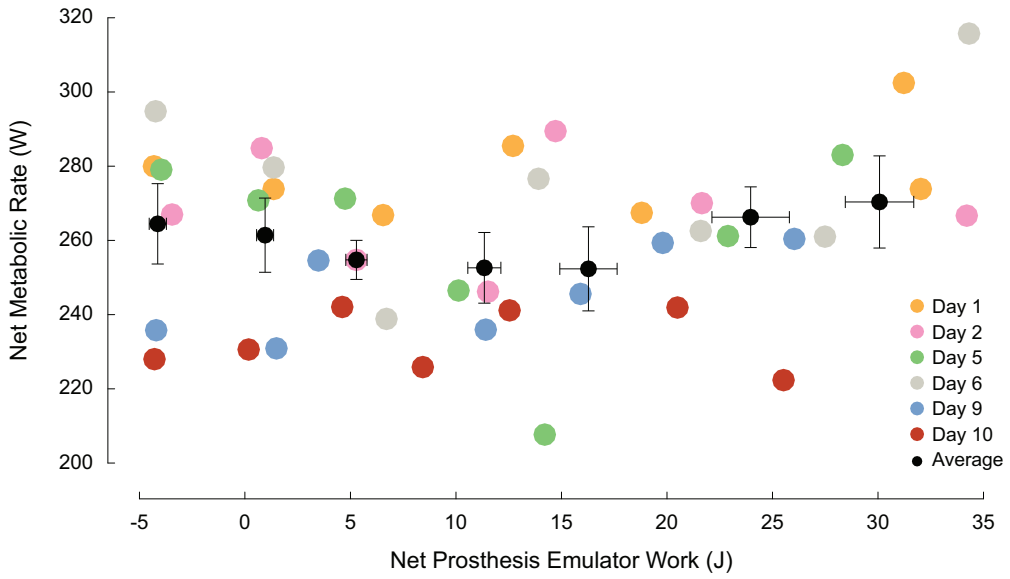

Figure S12: Metabolics data from six of ten data collections conducted with Subject 1. Over the course of all experiments, there appeared to be no relationship between metabolic rate and net prosthesis work rate. Data were collected at different times of the day, which may account for some of the variance in average metabolic rate per day. Mean data per condition are in black. Whiskers denote standard error in metabolic rate (vertical) and prosthesis work (horizontal).

References

Au, S. K., 2007. Powered Ankle-Foot Prosthesis for the Improvement of Amputee Walking Economy. Doctoral Dissertation, Massachusetts Institute of Technology.

Caputo, J. M. and Collins, S. H., 2014a. A universal ankle-foot prosthesis emulator for experiments during human locomotion. ASME Journal of Biomechanical Engineering 136, 035002.

Caputo, J. M. and Collins, S. H., 2014b. Prosthetic ankle push-off work reduces metabolic rate but not collision work in non-amputee walking. Nature Scientific Reports 4, 7213.

de Lava, P., 1996. Adjustments to Zatsiorsky-Seluyanov's segment inertia parameters. Journal of Biomechanics 29, 1223–1230.

Esposito, E. R., Whitehead, J. M. A., and Wiken, J. M., 2015. Step-to-step transition work during level and inclined walking using passive and powered ankle-foot prostheses. Prosthetics and Orthotics International, 0309364614564021.

Hawes, M. R., and Sovak, D., 1994. Quantitative morphology of the human foot in a North American population, Ergonomics, 37(7), 1213–1226.

Herr, H. M. and Grabowski, A. M., 2012. Bionic ankle-foot prosthesis normalizes walking gait for persons with leg amputation. Proceedings of the Royal Society of London B: Biological Sciences 279, 457–464.

Winter, D. A., 1991. The Biomechanics and Motor Control of Human Gait: Normal, Elderly and Pathological. Waterloo Biomechanics, Waterloo.

Zhang, J., Cheah, C. C., and Collins, S. H., 2015. Experimental comparison of torque control methods on an ankle exoskeleton during human walking. Proceedings of the IEEE International Conference on Robotics and Automation (ICRA), pages 5584-5589.